Detailed speciation of biomass pyrolysis products with a novel TGA-based methodology: the case-study of cellulose

Veronica Piazza [a], Roberto Batista da Silva Junior [a,1,2], Alessio Frassoldati [b], Luca Lietti [a], Stefano Chiaberge [c], Chiara Gambaro [c], Andrea Siviero [c], Tiziano Faravelli [b,*], Alessandra Beretta [a,*]

[a] *Laboratory of Catalysis and Catalytic Processes, Dipartimento di Energia, Politecnico di Milano, via La Masa 34, Milano 20156, Italy*
[b] *CRECK Modeling group, Dipartimento di Chimica, Materiali e Ingegneria Chimica, Politecnico di Milano, Piazza Leonardo da Vinci 32, Milano 20133, Italy*
[c] *ENI Novara Laboratories (CENTR), Via Giacomo Fauser, Novara 28100, Italy*

ARTICLE INFO

ABSTRACT

Pyrolysis of waste biomass represents a key route for the circular economy and a promising solution for the generation of valuable chemicals and liquid biofuels. The complex multi-component and multi-phase nature of the process, however, poses a challenge in acquiring comprehensive experimental data on biomass devolatilization. These data are essential for refining kinetic schemes and optimizing technology. This work presents a novel experimental methodology suitable for the collection of kinetically relevant data on biomass devolatilization combined with a complete characterization of the product slate. This methodology consists of a thermogravimetric analyser employed to carry out pyrolysis experiments, useful for the accurate monitoring of mass loss dependencies at varying heating rate, for the control of reaction temperatures and for the suppression of secondary gas-phase reactions as well as of transfer limitations. Multiple analytical methodologies and sampling protocols were combined for product speciation – downstream online MS for gases and H_2O, sorbing traps for integral offline GC–FID/MS measurement of heavy oxygenates, point vapour collection for instant GC–FID/MS analysis of light oxygenates – and allowed to independently determine the integral mass yield of each pyrolysis product, closing mass balances with very high accuracy. Experiments of cellulose pyrolysis at varying heating rate were carried out to tune and validate the methodology. Speciation protocols allowed to identify and individually quantify 31 species among pyrolysis products, including gases, condensable oxygenates, H_2O and char. The comparison of experimental findings with predictions from a state-of-art lumped model has highlighted the significance of the present methodology in unravelling the kinetics governing both devolatilization and product distribution.

1. Introduction

Bioenergy is an attracting solution within the current energy transition pursuing a gradual decrease of net-CO_2 production to contrast climate change. The existence of some critical issues, such as the competition with food production and extensive land uses is shifting the focus from conventional bioenergy sources to lignocellulosic biomass, which includes a vast variety of bioresources such as agricultural wastes, industrial organic waste streams and forestry residue [1]. The intrinsic variety of chemical composition among lignocellulosic biomass makes

thermal processes like combustion, gasification and pyrolysis the most suitable to "attack" by heat the biomass. Pyrolysis involves the thermal degradation of the starting biomass in an oxygen-free atmosphere with its conversion into a complex pool of products, that consists of gases (mainly CO, CO_2, H_2 but also C_xH_y), volatiles (C_1-C_7 oxygenates) and a carbonaceous solid residue called biochar. The yield of gas, liquid and solid streams can be tuned by changing the operating conditions, such as temperature, heating rate and residence time. The very first stage of biomass pyrolysis is the devolatilization, which identifies the release of primary vapour products from the starting solid biomass. These primary

products released in the gas phase can undergo secondary homogeneous reactions. While the knowledge on homogeneous kinetic schemes is well established, the comprehension on devolatilization chemistry, fundamental to improve the pyrolysis technologies and to develop modelling tools for the prediction of the behaviour of different feedstocks, remains an open challenge. In addition, comprehension of devolatilization mechanisms would be of great benefit for other thermal processes, like biomass gasification and combustion, where devolatilization still represents the very first conversion stage.

Thermogravimetric analysers (TGAs) represent a common tool to investigate the pyrolysis of biomass feedstocks at varying heating rates. Thermal stability is mostly influenced by the chemical composition of the starting biomass; consequently, the intrinsic complexity and variety of biomass feedstock has been significantly hindering the comprehension of devolatilization reactions. A possible strategy to approach in a structured way the study of biomass pyrolysis is to single out the behaviour of each macro-constituent: cellulose, hemicellulose and lignin [2–4]. Cellulose is a polysaccharide with linear chain of β (1→4) linked D-glucose units and is present in the form of microfibrils surrounded by hemicellulose chains and embedded in lignin regions [5]. Differently from cellulose, hemicellulose and lignin do not have a univocal chemical definition. Hemicellulose is a complex polymer where several sugar monomers are mixed (e.g. xylose, mannose, galactose, arabinose), while lignin is a macromolecule whose repeating units are hydroxycinnamoyl alcohols with different methoxylation degree. Pyrolysis experiments of the three macro-components in TGA have highlighted different devolatilization trends, with hemicellulose degrading at lower temperature when compared to cellulose and lignin being responsible for the highest solid yield [4,6,7]. This diverse behaviour proves the key role of the chemical nature of the starting biomass on thermal degradation pathways. For this reason, studying the devolatilization of each biomass constituent is a preliminary stage to subsequently explain and comprehend the behaviour of their mixtures and real biomasses [8].

Besides the study of thermal degradation trends, lab-scale methodologies have been designed to unravel the distribution of pyrolysis products. On one side, the coupling of TGA with analytical techniques such as TGA-FTIR, TGA-MS and EGA [9–13] has allowed to inspect pyrolysis gases and light vapours during the thermal evolution; however, the extreme complexity of the composition has been hindering the full characterization of the product slate. Instead, micro-pyrolyzers coupled with gas chromatography and mass spectrometry (Py-GC/MS) [14–17] and fixed-bed reactors [4,7,18] are the most common methodologies for the speciation of bio-oil; the use of lab-scale fluidized bed and conical spouted bed reactors has also been reported [19–23]. These approaches provide accurate information in terms of integral composition measurements, but they fail to capture the dynamics of devolatilization. Indeed, the complex multi-scale, multi-component and multi-phase nature of this process has been challenging the obtainment of fully informative data, with simultaneous characterization of devolatilization trends and quantitative speciation of the products.

Among the existing modelling tools which comprise the Flashchain, the FG-DVC and the CPD among others (see reference [24] and references therein), some of the authors have recently developed a multistep kinetic scheme, which consists of classes of reactions: i) solid pyrolysis and devolatilization; ii) char gasification and combustion; iii) secondary gas-phase reactions [25,26]. The kinetic scheme of biomass devolatilization (i) includes a set of lumped reactions and lumped species for each of three macro-components of biomass, cellulose, hemicellulose and lignin [25,27–31]. The model has been validated against a wide range of literature data gathered from diverse sources tested at different heating rates [28,30]. To enhance the accuracy of these kinetic schemes and transform them into increasingly reliable tools for technology optimization, expanding the sets of experimental data that provide insights in the pyrolysis kinetics is a key factor; besides, experiments need to mitigate heat and mass transfer limitations as well as the onset of secondary gas-phase reactions in order to provide the necessary information about the intrinsic kinetics of primary devolatilization.

This work aims to present a novel experimental methodology suitable for the collection of kinetically relevant data on biomass devolatilization: for this purpose, TGA was chosen as flexible and well-controlled setup, and it was improved to provide a complete quantitative speciation of pyrolysis products. In this context, it is essential to highlight that TGA experiments employ low heating rates. Therefore, it is recommended to conduct further analysis when applying kinetic data derived from this apparatus to model facilities where higher heating rates are used (e.g. industrial boilers, fast pyrolysis reactors) [32]. However, TGA measurements remain of key-relevance for inferring kinetic parameters of interest to simulate the devolatilization of biomass even under high-heating rate conditions. This aspect was demonstrated, for instance, by Lemaire et al. in [33], where thermogravimetric analyses were coupled with flat flame reactor measurements to infer proper kinetic parameters.

The experimental protocol was developed and validated by performing tests of cellulose pyrolysis, chosen as reference biomass for its extensive examination in current literature. In this respect, the lumped model served as a trace of the existing literature to guide the development of the methodology. Conversely, after validation of experimental procedures, the comparison of newly obtained experimental data with state-of-the-art models was used to highlight margins of improvement in current kinetic tools.

2. Material and methods

2.1. Modelling of cellulose pyrolysis

Modelling of cellulose pyrolysis tests was obtained by using the kinetic scheme proposed by Debiagi et al. [28], which describes cellulose devolatilization with lumped reactions and lumped species. In particular, the cellulose kinetic model includes three solid pseudo-species, that are cellulose (CELL, with $C_6H_{10}O_5$ molecular structure), activated cellulose (CELLA, $C_6H_{10}O_5$) and CHAR (pure-carbon species); in addition to these compounds, the computation of solid residue takes into account also metaplastic compounds (indicated as G{…} in the following), that are pseudo-species entrapped in the metaplastic phase before desorbing into the vapour phase at higher temperatures. Volatile compounds evolving in the vapour phase are lumped into 15 lumped species, including permanent gases (CO, CO_2, CH_4, H_2), condensable oxygenates (methanol, formic acid, formaldehyde, acetaldehyde, glyoxal, hydroxy-acetaldehyde, propanal, hydroxy-propanal, 5-hydroxymethyl-furfural, levoglucosan LVG) and H_2O. The details of the model are discussed elsewhere [27].

Table 1 shows the kinetic scheme, composed of 4 lumped reactions for cellulose devolatilization (R1-R4) and other 4 reactions for the release of metaplastic species (R5-R8) [28]. Apparent first-order rate laws are used and kinetic parameters (i.e. pre-exponential factors k_0 and activation energies E_a) are reported in Table 1.

The initial formation of intermediate active cellulose (R1) is taken into account, as widely suggested in the literature [34–38]. Two alternative routes are then used to describe the conversion of intermediate CELLA: as a first route, CELLA can decompose to levoglucosan LVG (R2), an anhydrosugar with formula $C_6H_{10}O_5$, or, alternatively, CELLA can fragmentate generating a pool of oxygenates with simultaneous release of gas species (R3); the global stoichiometry of fragmentation was developed by Debiagi et al. [28], based on an extensive bulk of published data from different sources. Devolatilization rate is governed by the CELLA formation reaction (R1), while R2/R3 ratio rules instead the distribution of pyrolysis products. A competitive route to CELLA formation is the direct CELL degradation reaction to CHAR and H_2O (R4).

Experiments carried out in TGA were simulated in OpenSMOKE++, a general framework for numerical simulations of reacting systems developed by some of the authors [39]. The lumped mechanism of cellulose pyrolysis was adopted inside a semi-batch reactor model, where

Table 1
Lumped kinetic mechanism of cellulose pyrolysis [28].

Reactions		Rate constants $k\left[\frac{1}{s}\right]$[**]
Cellulose devolatilization		
R1	CELL→CELLA	$1.5 \times 10^{14}\exp(-197/RT)$
R2	CELLA→LVG	$3.3 \times T\exp(-42/RT)$
R3	CELLA→0.40CH$_2$OHCHO+0.03CHOCHO+0.17CH$_3$CHO+0.25 C$_6$H$_6$O$_3$+0.35 C$_2$H$_5$CHO+0.20CH$_3$OH+0.15CH$_2$O+0.49CO+0.05 G{CO}+0.43CO$_2$+0.13 H$_2$+0.93 H$_2$O+0.05 G{COH$_2$}$_{LOOSE}$+0.02HCOOH+0.05CH$_2$OHCH$_2$CHO+0.05CH$_4$+0.1 G{H$_2$}+0.66CHAR	$2.5 \times 10^6\exp(-80/RT)$
R4	CELL→4.45 H$_2$O+5.45CHAR+0.12{COH$_2$}$_{STIFF}$+0.18 G{COH$_2$}$_{LOOSE}$+0.25 G{CO}+0.125 G{H$_2$}+0.125 H$_2$	$5 \times 10^7\exp(-130/RT)$
Metaplastic		
R5	G{CO}→CO	$5 \times 10^{12}\exp(-220/RT)$
R6	G{COH$_2$}$_{STIFF}$→0.2CHAR+0.2 H$_2$O+0.8CO+0.8 H$_2$	$1 \times 10^9\exp(-247/RT)$
R7	G{COH$_2$}$_{LOOSE}$→0.8CHAR+0.8 H$_2$O+0.2CO+0.2 H$_2$	$6 \times 10^{10}\exp(-209/RT)$
R8	G{H$_2$}→H$_2$	$1.8 \times 10^8\exp(-293/RT)$

[**] Rate constants $k\left[\frac{1}{s}\right] = k_0\left[\frac{1}{s \times K^n}\right] \times T^n\exp\left(-\frac{E_a\left[\frac{kJ}{mol}\right]}{RT}\right)$, with $R = 8.314\left[\frac{J}{mol \times K}\right]$

the biomass was modelled as a solid present in the reactor volume that devolatilizes, while vapour products leave the reactor. The temperature ramp for each simulation was specified as an input parameter.

2.2. Chemicals

Commercial microcrystalline cellulose powder (with an average particle size of 20 μm) was purchased from Sigma-Aldrich and used for pyrolysis experiments.

Levoglucosan (LVG, 1,6-Anhydro-β-D-glucose) analytical standard with a purity of 99% from Sigma-Aldrich was employed to calibrate the response factor of LVG in GC-FID. Acetone (HPLC Plus, purity ≥ 99.9%, Sigma-Aldrich) and 1-Fluoronaphthalene (purity 99%, Sigma-Aldrich) were respectively used as solvent and internal standard for liquid analyses in GC-FID. In addition, N,O-bis(trimethylsilyl)trifluoroacetamide (BSTFA, Sigma-Aldrich) and pyridine (Sigma-Aldrich) chemicals were used for derivatization of liquid samples.

2.3. Pyrolysis experiments in TGA

Experiments of cellulose pyrolysis were run in a thermogravimetric analyser (TGA, Hitachi STA7300 TG-DTA), where 5–30 mg of cellulose powders were placed in an open Pt sample pan (D = 5.2 mm, H = 2.5 mm) and an equivalent empty Pt-pan was used as reference for measurements. Selected tests performed with ceramic pans excluded a possible catalytic role of Pt. Before testing, TGA was kept under He flow at room temperature for sufficient time to ensure chamber evacuation; then, during pyrolysis tests the cellulose sample was subjected to a controlled heating ramp from room temperature up to 850 °C, while fluxing a controlled stream of He to drag pyrolysis vapours outside the TGA chamber soon after their formation, thus suppressing secondary gas-phase reactions. Experiments at different temperature ramps were performed, ranging from 3 °C/min to 100 °C/min. The flowrate of He was changed within the 75–285 NmL/min window depending on the specific goal of the experiment, as further illustrated in following sections. Experiments were repeated at least three times for each heating rate.

The TG curve (i.e. mass loss curve *Mass*) and the derivative mass loss curve (*DTG*), defined as in Eq.1 and Eq.2 respectively, were monitored during each test.

$$Mass \quad (T) = \frac{m_{cell}(T)}{m_{cell,0}} \times 100[\%] \tag{1}$$

$$DTG \quad (T) = -\frac{dMass(T)/100}{dt} \quad \left[\frac{1}{min}\right] \tag{2}$$

$m_{cell,0}$ and $m_{cell}(T)$ represent the initial mass of cellulose and the residual mass of cellulose present on the pan at temperature T, respectively. The *DTG* is calculated as the mathematical derivative of TG curve and is an indication of the release rate. DTA signal (differential thermal analysis signal, in μV) is also monitored as an indication of the endothermicity of the process.

In selected cases, at the end of pyrolysis experiment, the carrier gas was switched from He to air at 850 °C aiming to burn the organic solid residual in the pan after pyrolysis (i.e. biochar) and to have an indication of the ash content.

2.4. Analytical techniques

Multiple analytical techniques were combined for the identification and quantification of pyrolysis products.

A quadrupole mass spectrometer (HPR-20 EGA, Hidden Analytical) with SEM (Secondary Electron Multiplier) detector was connected to TGA-setup using a quartz inert capillary line (heated at 250 °C) and it was used for the online monitoring during pyrolysis experiments of gases and H$_2$O, as detailed subsequently.

Offline composition measurements of vapour and liquid samples of pyrolysis products were carried out in a GC-FID/MS instrument (Agilent 6890, 5973 MSD) provided with a HP-5MS capillary column (30 m x 250 μm x 0.25 μm). During the analysis, GC oven was kept at 40 °C for 5 minutes, heated up to 110 °C at 10 °C/min and then at 12 °C/min up to 300 °C. The column was operated at 6.6 psi using He as carrier gas and with a H$_2$/air ratio of (40 mL/min)/(400 mL/min) in FID detector. Injections were performed using syringes for liquid (1 μL sample) or gas (2 mL sample) to analyse liquid and vapour samples, respectively. Analyses in GC-MS were used to identify the species using a National Institute of Standards and Technology (NIST) mass spectral library, while the quantitative composition evaluation was based on GC-FID chromatograms. In addition, selected liquid samples were derivatized via silylation and analyzed in a GC-MS instrument (Thermo Finnigan Trace GC Ultra, Thermo Finninngan Trace DSQ MS) equipped with a capillary column SUPELCO MDN-5S.

2.5. Sampling of pyrolysis products

Sampling protocols for the collection of pyrolysis products were tuned for offline analysis in GC-MS/FID.

Samples of pyrolysis vapours were collected using a 2.5 mL gas syringe close to the outlet of the TGA chamber, where a sampling point (a T-connection) was placed. The vapour sample was collected during pyrolysis test, at the instant when cellulose reached 50% mass loss. It was then rapidly and manually injected into the offline GC-MS or GC-FID column. This differential sampling was taken as representative of the whole pool of species emitted during the devolatilization of cellulose, since its decomposition follows a one-step scheme, as explained in the following Section 3.1.

Orbo-609 (Supelco) traps were connected at the outlet of TGA chamber to entrap condensable pyrolysis products during pyrolysis tests: these traps are commercial sorbing tubes containing spheres of Amberlite XAD-2 resin and typically used for air quality monitoring. Each trap contains a "large bed" (400 mg, 50 mm) of sorbing spheres for products entrapping and a "short bed" (200 mg, 20 mm), used as backup to check for possible sample breakthrough. At the end of the experiments, the traps were removed from the line and sorbing spheres were poured into a vial, where 10 mL of acetone solution was then added to elute pyrolysis products. The acetone solution contained a known amount of 1-Fluoronaphthalene, used as internal standard for composition analysis (mother solution prepared with 10 µL of 1-Fluoronaphthalene in 250 mL of acetone).

3. Results and discussion

3.1. Development of a TGA-based methodology for complete speciation of pyrolysis products

The TGA-based experimental methodology was developed to reach an accurate quantitative speciation of pyrolysis products, being this of fundamental importance for the kinetic study and comprehension of the process. The collection, the identification and the quantification of pyrolysis products was challenged by the high number and large variety in the pool of species, that could be grouped as follows: H_2O, gas products, C_1-C_5 condensable products, C_{6+} condensable products, biochar. In the present setup, char was easily monitored in TGA (with an estimated uncertainty of $\pm 2.0\%$ yield), while further analytical methodologies and sampling procedures were implemented downwards the TGA chamber for the speciation of the other pyrolysis products. The large window of boiling temperature (from gases to LVG with a boiling temperature of ~385 °C) made the simultaneous capture and analysis of all classes of products unfeasible. To address this limitation a strategy based on adjusting the dilution of pyrolysis products in the gaseous stream was developed: tests were performed at different He carrier flowrates, based on the particular class of products under investigation, as detailed subsequently. Therefore, multiple experiments were carried out to fully determine product speciation for each cellulose pyrolysis condition.

Multiple analytical techniques were used to identify the multitude of products, and calibration protocols were developed to quantitatively determine the production of each single species. In this work, the product distribution is provided in terms of integral mass yields Y_i, defined as in Eq.3.

$$Y_i = \frac{m_i}{m_{cell,0}} \times 100 \, [\%] \tag{3}$$

Where m_i represents the total mass of the single species or the class of compounds i produced up to the end of the pyrolysis experiment. Since the integral mass yield of each pyrolysis product was calculated without forcing the closure of the mass balance, it was possible to check the goodness of species quantification by verifying the closure of the summation of mass yields.

While analytical instruments and sampling methods were presented in Sections 2.4 and 2.5, the full picture of the experimental setup and protocols is provided in this Section 3.1, with a detailed explanation of the approach to capture and quantify each class of pyrolysis products. Fig. 1 provides a graphical representation of the full TGA-based experimental protocol.

3.1.1. Speciation of C_{6+} compounds

Experiments for the analysis of C_{6+} compounds were carried out by connecting two in-series Orbo-609 traps at the outlet of TGA chamber to trap C_{6+} compounds released during pyrolysis. The employment of these traps, proposed also by Fabbri et al. in their study [40], has proved more effective for the capture of C_{6+} compounds than traditional cold traps. A high flowrate of He carrier (285 NmL/min) was used to dilute the stream, thus avoiding condensation of these heavy species in cold points before the traps. The traps were disconnected from the line at the end of the experiment. Then, the entire content of the first trap ("large bed" + "short bed") and the "large bed" of second one were poured into a vial and washed with 10 mL of acetone-based mother solution with 1-Fluoronaphthalene (described in Section 2.5) to elute pyrolysis products. The eluted solution was sampled with a liquid syringe and analysed in the offline GC/MS to identify the chemical structure of entrapped species. Chromatograms obtained in GC/MS were then coupled to analogous analyses in GC/FID for species quantification, such that it was possible to associate each peak to a single species. An example of chromatogram in GC/FID with species identification is reported in Fig. S1.1 of the Supplementary Material, paragraph S.1. A response factor for quantification of LVG was evaluated using 1-Fluoronaphthalene as internal standard: for the calibration, known amounts of LVG (solid at room temperature) were dissolved in known amounts of acetone solution with 1-Fluoronaphthalene and samples were injected in GC/FID. The response factor f_{LVG} was then evaluated using Eq.4, where $Area_{LVG}$ and $Area_{Fnapht}$ indicate the area below LVG and 1-Fluoronaphthalene peaks in GC/FID chromatograms, while $mmol_{LGA}$ and μL_{Fnapht} are their amount in the solutions used for calibration. The sensitivity of f_{LVG} was checked by repeating analyses at varying LVG concentration and an average value was calculated and used for experiments. Details about the f_{LVG} calibration procedure are reported in the Supplementary Material, paragraph S.2.

$$f_{LVG} = \frac{\left(\frac{mmol_{LVG}}{\mu L_{Fnapht}}\right)}{\left(\frac{Area_{LVG}}{Area_{Fnapht}}\right)} = 0.028 \tag{4}$$

This same response factor was used for the quantification of the other C_{6+} compounds, a reasonable assumption due to the similarity of their chemical structure with that of LVG.

The use of GC/FID and of the calibrated response factor allowed to quantify the integral moles of each species captured in traps during pyrolysis experiments, and, therefore, to estimate their individual integral mass yield Y_i (Eq.3). An uncertainty of $\pm 2.7\%$ yield was estimated for LVG. Moreover, LVG quantification was also checked with ad-hoc measurements after silylation, that proved the validity of the present quantification protocol.

This speciation protocol was used exclusively for C_{6+} compounds, while different procedures were developed for C_1-C_5 oxygenates, gases and H_2O.

3.1.2. Speciation of C_1-C_5 species

Pyrolysis vapours were sampled at the outlet of TG chamber (stream (1) in Fig. 1) for the speciation of C_1-C_5 compounds. As a first step, the vapour sample was injected in GC/MS for species identification; a second experiment was then run for injection and quantification in GC/FID. Following the same approach adopted for the analysis of the liquid sample, the peaks observed in the two chromatograms were coupled; an
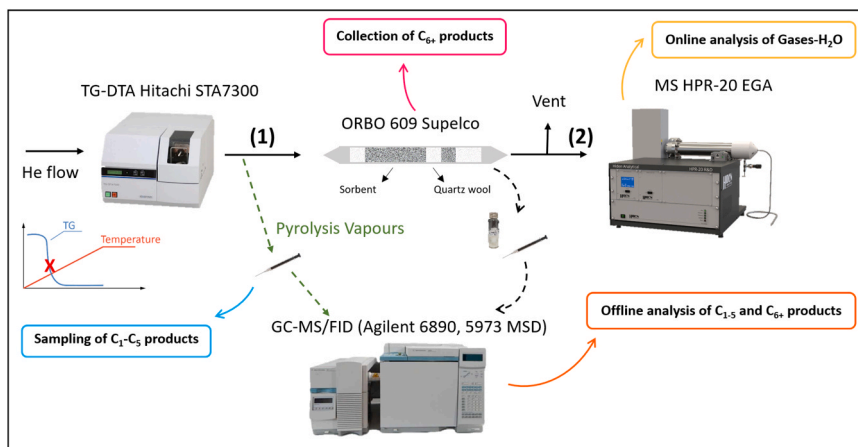
Fig. 1. TGA-based methodology for biomass pyrolysis tests with complete product speciation.

example of GC/FID chromatogram is reported Fig.S3.1 of the Supplementary Material, paragraph S.3. For these experiments He flowrate was lowered to 75 NmL/min to avoid excessive dilution of pyrolysis products in the vapour mixture that could compromise composition analyses; it is important to underline that partial condensation of levoglucosan in the line upwards the sampling point due do the reduced He flowrate was observed, but, as explained in paragraph 3.1.1, the quantification of C_{6+} compounds was carried out independently with ad-hoc experiments.

As widely recognized in literature, cellulose pyrolysis takes place in a single-step devolatilization [41–44]; thus, reasonably, the point composition analysis could be taken as representative as integral production of each species. For quantification purposes, levoglucosenone (LGO), one of the C_6 anhydrosugars produced in cellulose pyrolysis and quantified in the Orbo-609 traps, was chosen as internal standard. Indeed, unlike LVG, it was possible to fully capture LGO in vapour sampling, being its boiling temperature significantly lower (231 °C of LGO vs 385 °C of LVG). Therefore, the following correlation is used to estimate the integral mass yield of each of C_1-C_5 compounds (Eq.5).

$$Y_i = \left(\frac{Area_i}{Area_{LGO}} \right) Y_{LGO} \left(\frac{MM_i}{MM_{LGO}} \right) \times 100 [\%] \quad (5)$$

Where MM_i and MM_{LGO} indicate the molar mass of a generic species i and of LGO, respectively.

3.1.3. Speciation of gases and H_2O

Gases (CO, CO_2 and CH_4) and H_2O were monitored and quantified by online MS downwards Orbo-609 traps (stream (2) in Fig. 1). He carrier flowrate was set as 285 NmL/min, which allowed to reach feasible concentration level for MS analyses while minimizing the dead time between dynamics of TGA chamber and the detection by MS, due to the time required to pass through the traps and the transfer line. In particular, a time lag of 12 s was measured and it was taken into account for the graphical representation of MS signals. Despite of the relatively long residence time in the transfer line, the high level of dilution and the low temperature of the stream prevent any secondary gas-phase reactions of the products released during pyrolysis.

Proper calibration factors were tuned to estimate concentration values from MS signals. For this purpose, calibration factors were evaluated by sending stream with known concentration of CO_2 and H_2O to the MS instrument and were defined as in Eqs.6–9, where *molar fraction i* and SEM_i indicate the concentration chosen for the calibration and the signal produced by MS detector (after baseline subtraction) for i fragment, respectively. It is seen that fragment $m/z = 18$ was used for H_2O monitoring and $m/z = 44$ for CO_2; the quantification of CH_4 (fragment $m/z = 15$) and CO (fragment $m/z = 28$ after subtraction of contribution from CO_2) was simplified by assuming the

same calibration factor as CO_2.

$$\alpha_{H_2O} = \frac{molar\ fraction\ H_2O}{SEM_{18}} = 1.5 \times 10^6 \quad (6)$$

$$\alpha_{CO_2} = \frac{molar\ fraction\ CO_2}{SEM_{44}} = 1.9 \times 10^6 \quad (7)$$

$$\alpha_{CO} = \frac{molar\ fraction\ CO}{SEM_{28} - 0.098 \bullet SEM_{44}} = \alpha_{CO_2} \quad (8)$$

$$\alpha_{CH_4} = \frac{molar\ fraction\ CH_4}{SEM_{15}} = \alpha_{CO_2} \quad (9)$$

Only CO, CO_2, H_2O and CH_4 species were detected and followed in online MS during pyrolysis experiments; their integral production was evaluated to estimate their integral mass yields Y_i (Eq.3) and to verify mass balances. An uncertainty of ± 0.6%, ± 0.9% and ± 2.3% yield were estimated for CO, CO_2 and H_2O, respectively.

3.2. Devolatilization kinetics from TGA tests

Before addressing the speciation of pyrolysis products, the goodness of TGA setup was assessed by performing cellulose pyrolysis experiments at varying heating rates, and by comparing the measured mass loss trends with the current scientific literature as well as with predictions of the state-of-art lumped model described in Section 2.1.

3.2.1. Thermal analysis at varying heating rate

Pyrolysis experiments were performed at varying heating rate, ranging from 3 °C/min up to 100 °C/min. In Fig. 2, TG, DTG, and DTA data are presented and reveal that the pyrolysis of cellulose occurs through a one-step devolatilization process. This step is characterized by a rapid loss of weight within the temperature range of 250–450 °C, which is consistent with the findings reported in the existing literature [41–44]. Before the onset of the main devolatilization step, a slow decrease of cellulose mass is observed, lowering down to 97.7/98.9% at 220 °C and indicating the gradual release of moisture. Consistently, DTG curves in Fig. 2C show a mass-loss stage centred at 200 °C. Above 450 °C, TG curves flatten down to a value of approximately 8%, which represents the solid residue after cellulose pyrolysis, including both biochar and ashes. A minor ash content of 0.2 wt% was quantified by burning char with air at 850 °C.

TG curves in Fig. 2A indicate a shift of the pyrolysis to higher temperatures with increasing heating rates, which is a well-known dynamic effect [45,46]. This trend in cellulose thermal stability can be also appreciated by looking at the location of DTG peak maximum in Fig. 2C, which shifts from 340 °C for the test conducted at 10 °C/min to 354 °C at
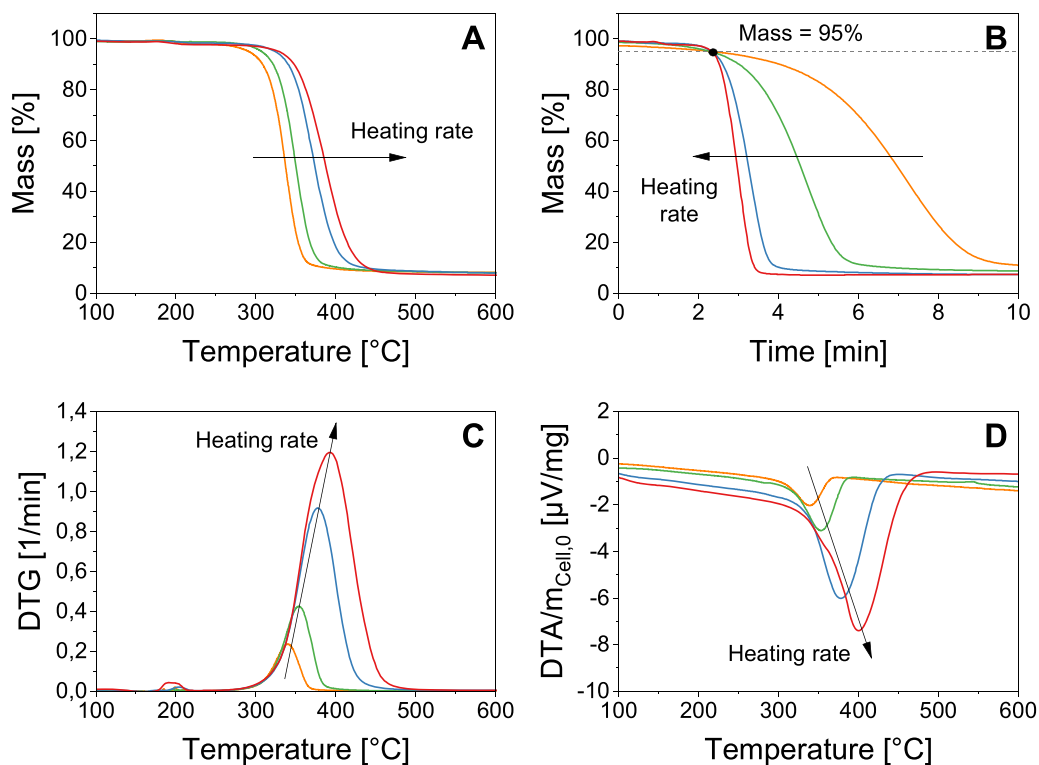
Fig. 2. Effect of heating rate on TG (A-B), DTG (C) and DTA (D) during cellulose pyrolysis. Orange: 10 °C/min – green: 20 °C/min – blue: 60 °C/min – red: 100 °C/min.

20 °C/min, to 377 °C at 60 °C/min and finally to 392 °C at 100 °C/min. Moreover, Fig. 2B clearly shows that the duration of the devolatilization shortens with the increase of heating rate: during experiment at 10 °C/min devolatilization takes place within a ~6.5 min interval, while at 100 °C/min cellulose quickly decomposes with an intensive pulse-like release of pyrolysis products [47]. For this reason, the intensity of DTG peak is higher for experiments at higher heating rate, whose duration was lower (Fig. 2C). In the same way, the DTA curves (normalized by the initial cellulose mass for a correct comparison in Fig. 2D) exhibit minima at temperatures coinciding with the DTG peaks.

A slight impact of heating rates is also noticed on the solid residual, moving from 9.0% at 10 °C/min to 7.3% at 100 °C/min (Fig. 2A). Indeed, the positive effect on biochar yield of a prolonged preheating of lignocellulosic biomass at low temperature (250–300 °C), has been extensively observed in the literature [48,49]. This behaviour can be explained by the promotion of cellulose carbonization (with dehydration and inter-/intra-molecular cross-linking reactions), leading to a rearranged structure of cellulose polymer chains and to the formation of an aromatic polycyclic network with increased organization and thermal stability [50–52].

It was verified that the insertion of Orbo-609 traps downstream of the TGA did not affect TG curves, as well as the choice of He flowrate and initial cellulose mass. The 100 mg•°C/min threshold recommended by ICTAT [53] was exceeded in many tests of this work. Indeed, higher biomass weights were beneficial to maximize the concentration of eluted volatiles and benefit composition analysis. It was observed that devolatilization trends largely coincided, affirming their kinetic relevance. In this respect, an extended set of experimental results is reported in Fig. S4.1 and Fig. S4.2 of the Supplementary Material, paragraph S.4.

Experimental results collected in TGA were used for the evaluation of an apparent activation energy $E_{a,app}$ for cellulose pyrolysis, using the Ozawa-Flynn-Wall (OFW) iso-conversion model-free method [54–58].

The $E_{a,app}$ was calculated using experimental data at conversion in the 10–60% range and multiple heating rates (3–10-20 °C/min). An average apparent activation energy of 172 kJ/mol with a 95% confi-

dence interval of ± 12 kJ/mol was estimated for the commercial microcrystalline cellulose used in the present study, in agreement with the range of values reported in the literature [45]. Details about the OFW equations, Arrhenius plots of iso-conversional curves and fitting results are reported in the Supplementary Material, paragraph S.5.

3.2.2. Model predictions of TG
Experimental TG curves are compared with model predictions in Fig. 3, where simulations were performed considering a dry ash-free cellulose. The model well predicts the mass loss trend as well as the solid residue, despite a slight shift at higher temperatures for all the tested heating ramps. The CELLA formation reaction (R1) in the lumped kinetic scheme is the one controlling the predicted TG curve and, interestingly, its activation energy (197 J/mol, Table 1) is slightly higher than the $E_{a,app}$ of 172 kJ/mol estimated from measured TG curves. This value of 197 kJ/mol corresponds to the most probable $E_{a,app}$ for cellulose pyrolysis proposed by Broadbelt et al. in [59], in agreement with their mechanistic model. Indeed, kinetic parameters of the lumped model were derived by fitting an extensive set of published TGA data, collected with celluloses of diverse nature and ranging from heating rate as low as 1 °C/min up to 1000 °C/s [60]. The difference between this generalized value of activation energy and the $E_{a,app}$ of the specific microcrystalline cellulose employed in the present work can explain the gap between experimental and predicted values.

As expected, by setting the activation energy of CELLA formation reaction at the measured apparent $E_{a,app}$, and by tuning the pre-exponential factors of this reaction (R1) and of CHAR formation reaction (R4) against the whole set of experimental TG data, a very accurate simulation could be obtained. Modified parameter estimates for the commercial cellulose herein studied are reported in Table 2, while Fig. 3 reveals the good agreement of the revised kinetics with experimental data. In addition, Arrhenius plots for original and modified kinetics are compared in Fig.S6.1 in the Supplementary Material, paragraph S.6.

This procedure has enabled a refinement of the general model for the
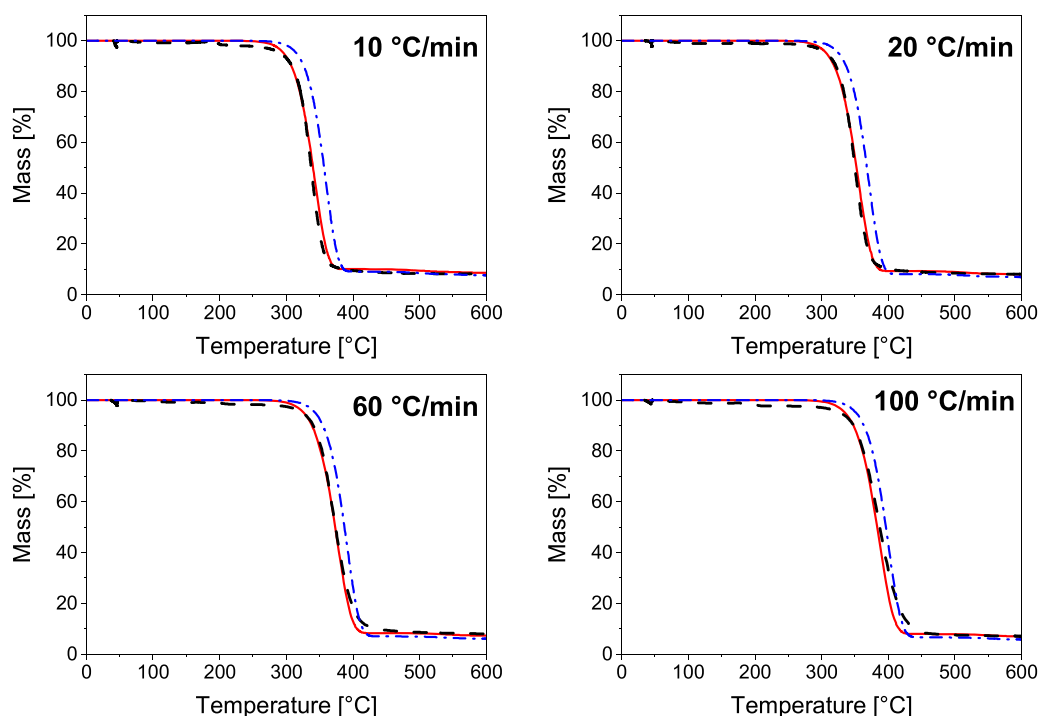
Fig. 3. TG curves in cellulose pyrolysis at varying heating rate: experimental measurements (black dashed lines), predictions from general model (blue dash-dotted lines) and from modified model (red solid lines).

Table 2
Modified kinetic parameters of *CELL* devolatilization reactions.

Reactions	Rate constants $k\left[\frac{1}{s}\right]$ **
R1	$3.0 \times 10^{12} \exp\left(-\frac{172}{RT}\right)$
R4	$1.2 \times 10^{8} \exp\left(-\frac{130}{RT}\right)$

**Rate constants $k\left[\frac{1}{s}\right] = k_0\left[\frac{1}{s \times K^n}\right] \times T^n \exp\left(-\frac{E_a\left[\frac{kJ}{mol}\right]}{RT}\right)$, with $R = 8.314\left[\frac{J}{mol \times K}\right]$

Table 3
Integral yields of cellulose pyrolysis products: macro-groups and mass balance.

	Integral mass yield (wt%) 20 °C/min	Integral mass yield (wt%) 100 °C/min
Gases	3.2	4.4
Water	10.2	5.8
Bio-oil$_{WF}$	78.8	85.0
Char	6.3	5.1
Ash	0.2	0.2
Total	**98.7**	**100.5**

specific cellulose herein investigated; in turn, this methodology allowed to align model predictions to the measured TG-dynamics for a more consistent comparison between experimental and predicted product speciation, as shown in the following sections.

3.3. Detailed product speciation

3.3.1. Measured yields at varying heating rate

The detailed qualitative and quantitative analysis of products obtained from cellulose pyrolysis at 20 °C/min and 100 °C/min was carried out following the procedures presented in Section 3.1. The product distribution is expressed in the form of integral mass yields of each gas species, of each condensable compound and of solid residue, and the effectiveness of the experimental protocol was verified by the closure of mass balance and the comparison with the available literature. Table 3 reports mass yields of product streams (gases, water, bio-oil, biochar and ash), where the term "bio-oil$_{WF}$" ("water-free bio-oil") indicates the condensable organic products and does not include H_2O.

Firstly, it is important to underline that impressive mass balances were obtained, with the summation of integral mass yields closing to

98.8% and 100.5% for the two sets of experiments at 20 and 100 °C/min, respectively. This represents an unparalleled finding since, at the best of the authors' knowledge, this is the first time that a TGA-based setup has successfully provided a complete and accurate quantification of the entire product slate. This direct coupling of mass loss measurements in micro-balance with full products speciation allows to collect at the same time kinetically informative data on both apparent activation energies and product distribution.

The majority of cellulose conversion during the experiment at a heating rate of 20 °C/min can be attributed to condensable products, which include both H_2O and organic species. These products account for a significant portion of the conversion, with a total mass yield of 10.2% for H_2O and 78.8% for bio-oil$_{WF}$. In contrast, the mass yields of gases and solid residue are limited to 3.2% and 6.5%, respectively. Similar results are observed at the higher heating ramp of 100 °C/min, even if a higher yield of bio-oil$_{WF}$ was reached (85.0%) at the expense of H_2O (5.8%). Similar distributions are observed in the literature, where cellulose is known to maximize the yield of the liquid fraction: yields of 4.6%, 83.2%, 6.9% and 5.4% to char, organic bio-oil, H_2O and gases, respectively, were observed during cellulose pyrolysis in micropyrolyzer at 500 °C by Zhou et al. [17], and similar results are presented by Ansari et al. for thin-film fast pyrolysis experiments [61]. Instead, experiments carried out in fixed bed reactors showed a lower yield of liquid fraction (65–70% at 500 °C) [4,62], possibly due to the impact of transfer limitations or secondary reactions.

Table 4 shows integral mass yields of each single detected compound. Carbon monoxide and carbon dioxide were the main gas products, as widely confirmed in the literature [3,47,51,63]. Traces of CH_4 were also observed at 100 °C/min, whereas it was not detected at 20 °C/min, likely because the increased dilution in the vapor stream (due to the longer duration of the test) caused it to fall below the detectability limit of MS detector. No measurable H_2 production was observed.

A wide range of oxygenated species is present in the organic bio-oil phase, comprising anhydrosugars, monosaccharides, furanic species, linear ketones and aldehydes. Levoglucosan represents by far the most important product, accounting for 54.2% and 47.6% of integral yield at 20 and 100 °C/min, respectively. Similar yields were observed in micropyrolyzer tests at 500 °C [17,64,65]. Levoglucosan is originated from the initial depolymerization of cellulose chains with the cleavage of the 1,4-glycosidic bond and successive intramolecular rearrangement, as widely clarified in the literature [47,66]. Other C_6 anhydrosugars (Levoglucosenone LGO, 1,4:3,6-dianhydro-α-D-glucopyranose DGP, 1, 6-anhydro-β-D-glucofuranose AGF, 3,4-Anhydro-d-galactosan, 2, 3-Anhydro-d-mannosan), the monosaccharides D-Allose and the glucose analogue 2-Deoxy-D-galactose were detected. The formation of these anhydrosugars and simple sugars shares the same initiation step of levoglucosan formation (i.e. release of hydroxyl radical) but further chemical structure rearrangements must then take place before monomer release, thus making the formation of levoglucosan significantly favoured [47]. Traces of DL-Arabinose, a pentose sugar, are also detected, probably resulting from the contamination of starting cellulose chains with hemicellulose-like monomers.

Furan-derived species, mostly furan, 2-methylfuran and furfural, represent another important class of condensable species produced from cellulose pyrolysis. A direct route to furanic species from cellulose chain has been proposed in the literature [47,67], passing through the ring opening of the polymeric unit initiated by the cleavage of the ring glycosidic bond to form a linear C_6 aldehyde. After dehydration and an intramolecular acetal reaction, 5-Hydroxymethylfurfural (5-HMF) is expected to be produced as primary product [47]. Remarkably, 5-HMF was not detected in the present work: this evidence suggests that 5-HMF decomposition routes to other furanic species can take place before devolatilization, in the pseudo-liquid phase formed during cellulose pyrolysis [68,69]. Low 5-HMF productivity (~ 0.6–1.3% yield) were recently observed in micropyrolyzer tests, even if it remained the most abundant furanic product [64,65].

Linear ketones and aldehydes with short carbon chain were also produced, among which formaldehyde, acetaldehyde, acetone and 2,3-butanedione share higher yields. Similar species and productivities were observed in recent works based on micropyrolyzer experiments [17,61]. Shen et al. showed that both direct fragmentation routes from cellulose polymer and secondary gas-phase reactions can be recalled to explain the production of this class of compounds [47]. In this view, the present experimental setup could be of great value to isolate the contribution of primary devolatilization reactions.

Fig. 4 plots integral mass yields of class of compounds evaluated at 20 and 100 °C/min, in order to visualize the effect of heating rate on the product distribution obtained from cellulose pyrolysis. In Fig. 4A, besides gases, char and H_2O, oxygenated species were grouped according to the number of C-atoms in their molecule (C_{1-7}). As already explained, similar features are seen in the two cases, with the distinct standing out of C_6 species and in particular levoglucosan. In the test at 100 °C/min species other than levoglucosan are detected in larger amount, for all the classes: C_1 (Formaldehyde), C_2 (Acetaldehyde), C_3 (Acetone, Hydroxyacetone), C_4 (Furan, Butanedione) and C_5 (Methylfuran, Glutaraldehyde). Indeed, when operating at 100 °C/min biomass devolatilization takes place at higher temperature (as shown by DTG plots in Fig. 2C) and this favours those pathways that compete with the simple release of the monomeric levoglucosan unit. Consistently, species other than anhydrosugars like furanic species, aldehydes and ketones gain importance

during tests at 100 °C/min, as shown in Fig. 4B.

3.3.2. Model predictions of product distribution

The proposed experimental protocol has proven its suitability to outline product speciation with a level of accuracy way higher with respect to state-of-art lumped model predictions, being the number of detected pyrolysis products the first indication: 31 species were identified and quantified during experiments, while the lumped model (described in Section 2.1) describes cellulose devolatilization using only 16 compounds. In this paragraph, measured product speciation is compared with predictions from the lumped scheme aiming to identify potential limitations of existing kinetic models and to pave the way for additional improvements and refinements.

3.3.2.1. Integral mass yields. Fig. 5 shows the comparison between measured and predicted integral mass yields of different classes of compounds, grouped according to the C-chain length (Fig. 5A) or their chemical functionality (Fig. 5B), observed in cellulose pyrolysis at 100 °C/min.

Char production predicted by the model is fully in line with the experimental evidence, while the kinetic routes to H_2O and gases (4.8% yield of CO, 5.3% of CO_2, and only 0.1% of H_2 and 0.2% of CH_4) in the lumped scheme appears overestimated. In both cases levoglucosan represents by far the most important product (with 47.6% yield in the experiment and 44.7% according to the model), while the greatest discrepancy has emerged in the definition of the distribution among other C_2-C_5 oxygenates. Indeed, the experiments were able to better define the entire range of products with respect to the model, where for instance species C_4, C_5 and C_7 are missing. Moreover, experimental results prove a higher yield to anhydrosugars/sugar monomers, while an opposite situation is seen for aliphatic aldehydes/ketones. This trend confirms that the experimental set-up allowed to capture primary products from the cleavage of cellulose polymeric chain bonds, before further fragmentation reactions into smaller compounds. This capability of the present experimental protocol to detect and quantify the entire product slate appears as of significant importance for the refinement of kinetic models of biomass primary devolatilization reactions. As a preliminary observation, the lumped model appears to overestimate the route to lighter oxygenates (reaction R3 in Table 1) in competition with anhydrosugar formation (reaction R2).

3.3.2.2. Dynamic evolution of gases and H_2O. Besides integral productivities, the present TGA-setup allowed to follow the dynamic evolution of gases and H_2O. Experimental measurements (red lines) of CO, CO_2 and H_2O flowrates are compared with model predictions (green dashed lines) in Fig. 6. The production of these species well fits with the biomass mass loss during devolatilization, such that their peak flowrate matches with the center of mass loss curve. All the species show a trend with a maximum, consistently with the hypothesis of single step devolatilization taking place during cellulose pyrolysis. Fig. 6 shows that the experimental peak of H_2O is not symmetrical and presents a tail at higher temperatures: this behavior is explained by the delay provoked by Orbo traps, which partially block H_2O flow.
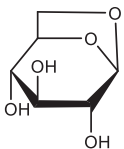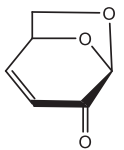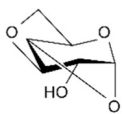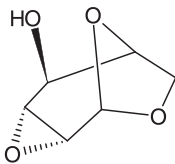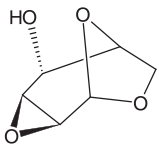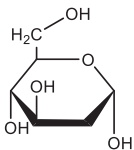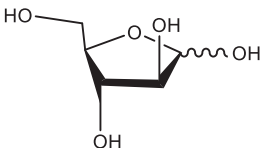
As expected by the comparison of integral yields (Fig. 5), the model overestimates the production of all the species, H_2O, CO and CO_2. Moreover, a second peak of CO is predicted by the model at higher temperature (520 °C), due to the delayed release of metaplastic species (R5-R8 in Table 1). This phenomenon appears as overemphasized by the model, since this second contribution is not revealed during the experiment.

4. Conclusions

This study presents a novel and flexible TGA-based methodology that combines the obtainment of kinetically relevant data on biomass
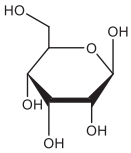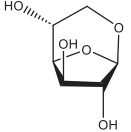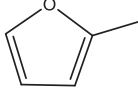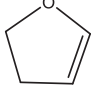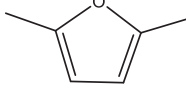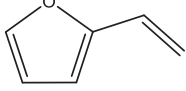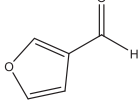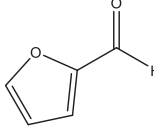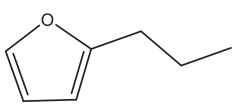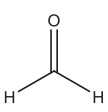
Table 4
Integral yields of cellulose pyrolysis products: single species.

	Formula	Molecular structure	Integral mass yield (wt%) 20 °C/min	Integral mass yield (wt%) 100 °C/min
Gases				
Carbon monoxide	CO		1.0	1.7
Carbon dioxide	CO_2		2.2	2.5
Methane	CH_4		-	0.2
Anhydrosugars, monosaccharides				
Levoglucosan (LVG)	$C_6H_{10}O_5$		54.2	47.6
Levoglucosenone (LGO)	$C_6H_6O_3$		3.6	1.5
1,4:3,6-dianhydro-α-D-glucopyranose (DGP)	$C_6H_8O_4$		2.3	1.4
3,4-Anhydro-d-galactosan	$C_6H_8O_4$		0.9	0.6
2,3-Anhydro-d-mannosan	$C_6H_8O_4$		0.8	0.9
2-Deoxy-D-galactose	$C_6H_{12}O_5$		3.1	3.6
DL-Arabinose	$C_5H_{10}O_5$		0.2	0.1
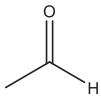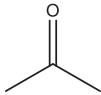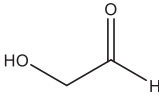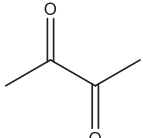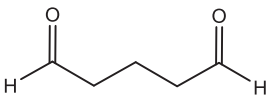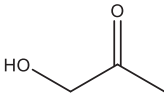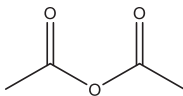
Table 4 (*continued*)

	Formula	Molecular structure	Integral mass yield (wt%) 20 °C/min	Integral mass yield (wt%) 100 °C/min
D-Allose	$C_6H_{12}O_6$		0.9	0.8
1,6-anhydro-β-D-glucofuranose (AGF)	$C_6H_{10}O_5$		4.0	3.8
Furans				
Furan	C_4H_4O		2.1	4.6
2-methylfuran	C_5H_6O		1.2	2.2
2,3-dihydrofuran	C_4H_6O		-	0.5
2,5-dimethylfuran	C_6H_8O		-	0.6
2-Vinylfuran	C_6H_6O		-	0.4
3-Furaldehyde	$C_5H_4O_2$		-	0.3
Furfural	$C_5H_4O_2$		2.8	2.4
2-propylfuran	$C_7H_{10}O$		0.9	0.9
Ketones, aldehydes				
Formaldehyde	CH_2O		0.1	1.2

Table 4 (*continued*)

	Formula	Molecular structure	Integral mass yield (wt%) 20 °C/min	Integral mass yield (wt%) 100 °C/min
Acetaldehyde	C_2H_4O		0.3	1.7
Acetone	C_3H_6O		1.0	3.9
Hydroxy-acetaldehyde (HAA)	$C_2H_4O_2$		-	0.7
2,3 Butanedione	$C_4H_6O_2$		0.2	2.4
Glutaraldehyde	$C_5H_8O_2$		-	0.2
Hydroxy-acetone	$C_3H_6O_2$		-	0.4
Others Cyclopentadiene	C_5H_6		0.1	1.4
Acetic anhydride	$C_4H_6O_3$		-	1.1
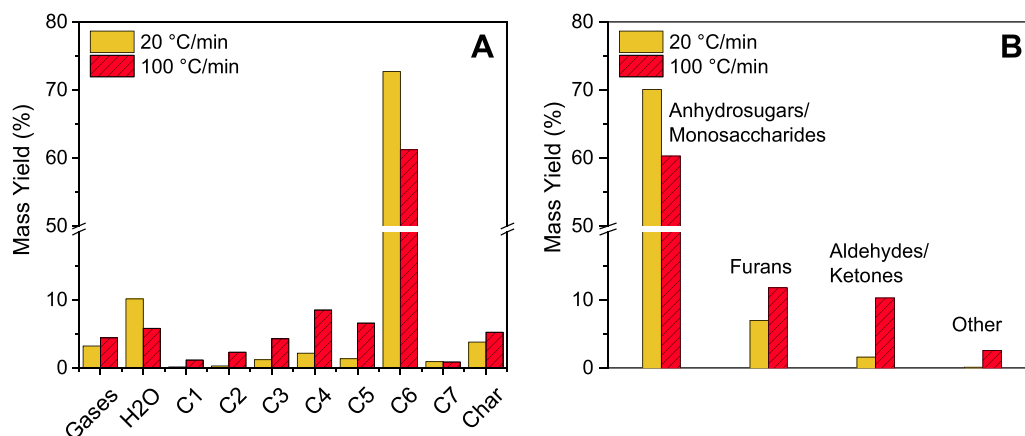
Fig. 4. Integral mass yields of different classes of compounds in cellulose pyrolysis experiments.

devolatilization with a complete identification and quantification of pyrolysis products. The direct coupling of thermal measurements in TGA with complete product speciation represents a notable result for the development of kinetic tools. Indeed, this methodology allows to collect with a single experiment informative data both on devolatilization kinetics (e.g. apparent activation energies of devolatilization) and on kinetic dependences responsible for product distribution.

Tests were performed in a TGA, where the biomass sample was

Fig. 5. Integral mass yields in cellulose pyrolysis at 100 °C/min: experimental (red) and modelling (green) results. Number of species in the range C_x-C_y is also reported on the right panel.

Fig. 6. TG trend and molar flows of CO, CO_2 and H_2O during cellulose pyrolysis at 20 °C/min: experimental measurements (red) vs model prediction (green dashed).
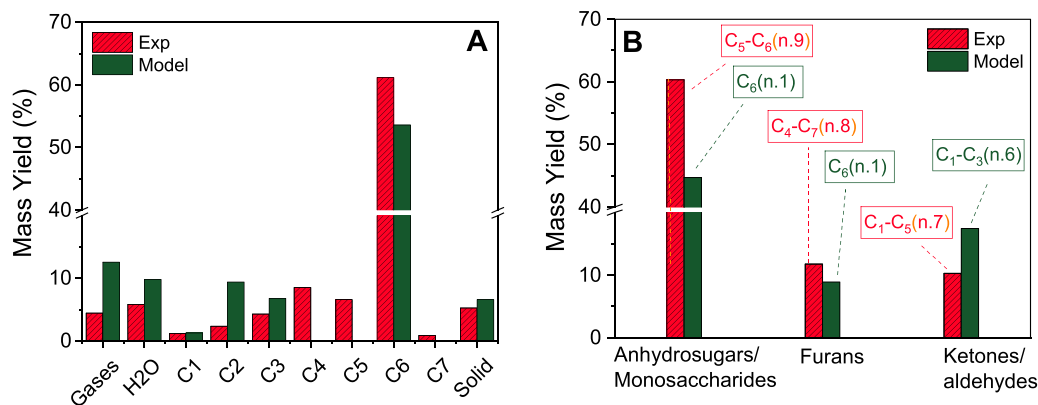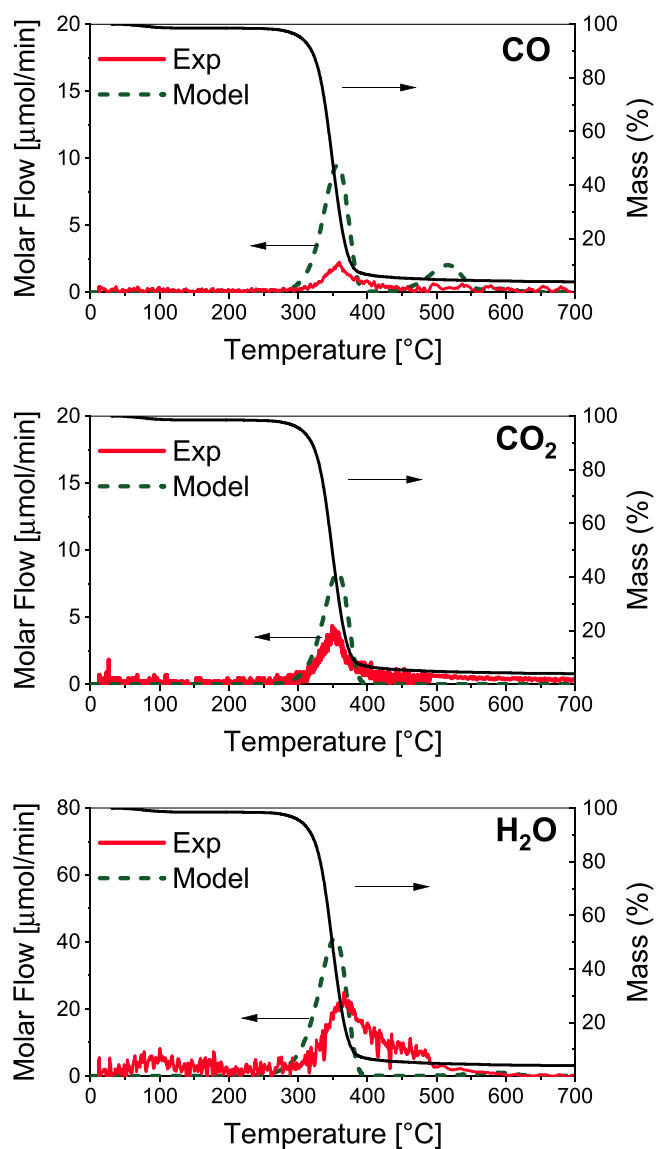
subjected to a controlled heating rate under a continuous He flow. Sample temperature and mass loss were monitored during the test, and residue char was easily measured. Multiple analytical techniques and sampling protocols were then combined to identify the multitude of products and calibration protocols allowed to quantitatively determine the production of each single species. In particular, online MS was used for monitoring light gases and H_2O, heavier products were entrapped in commercial sorbing traps and analysed integrally at the end of each test, and samples of the pyrolysis vapours were also taken to detect light oxygenates.

Experiments of cellulose pyrolysis at varying heating rates were performed to tune the methodology. Analysing the impact of heating rate, and consequently, temperature, on both mass loss curves and product distribution, provided a deeper understanding of cellulose pyrolysis phenomena. This examination yielded valuable insights that are beneficial for enhancing kinetic models.

A published lumped model served as a trace of the existing literature to guide the development of the experimental protocol. After validation of the approach and verification of the good agreement with state-of-the-art knowledge (e.g. single-step devolatilization process, massive production of levoglucosan), newly collected experimental data were used to highlight possible margins of improvement of available kinetic tools. The investigation showed that, while mass loss trends are well predicted by the available model, important margins of improvement in terms of product speciation are present, in particular in the definition of light oxygenates (C_2-C_5) production.

In conclusion, the experimental methodology developed in this study has proven to be a valuable, versatile, and highly effective solution for collecting essential kinetic data required to understand devolatilization chemistry and improve the modelling tools. This achievement is highly significant considering that the development of analytical devices based on thermogravimetric analyses (despite the limitations associated to these instruments, e.g. low heating rates) should be pursued to derive information on reaction kinetics and mechanism, which are of great benefit for all thermal processes – pyrolysis, gasification, combustion – where devolatilization still represents the very first conversion stage of the biomass.

CRediT authorship contribution statement

Veronica Piazza: Investigation, Data Curation, Methodology, Writing – Original Draft. **Roberto Batista da Silva Junior:** Supervision, Investigation, Methodology. **Alessio Frassoldati:** Supervision, Writing - review & editing. **Luca Lietti:** Supervision, Methodology, Writing - review & editing. **Stefano Chiaberge:** Methodology, Supervision. **Chiara Gambaro:** Conceptualization, Supervision, Funding acquisition. **Andrea Siviero:** Investigation, Methodology. **Tiziano Faravelli:**

Supervision, Conceptualization, Writing - review & editing. **Alessandra Beretta:** Supervision, Conceptualization, Methodology, Visualization, Funding acquisition, Writing - review & editing.

Declaration of Competing Interest

The authors declare that they have no known competing financial interests or personal relationships that could have appeared to influence the work reported in this paper.

Data availability

Data will be made available on request.

Acknowledgements

Appendix A. Supporting information

Supplementary data associated with this article can be found in the online version at doi:10.1016/j.jaap.2024.106413.

References

[1] IEA - International Energy Agency, World Energy Outlook 2022, 2022. www.iea. org/t&c/ (visited in May 2023).

[2] J. Yu, N. Paterson, J. Blamey, M. Millan, Cellulose, xylan and lignin interactions during pyrolysis of lignocellulosic biomass, Fuel 191 (2017) 140–149, https://doi. org/10.1016/j.fuel.2016.11.057.

[3] V. Pasangulapati, K.D. Ramachandriya, A. Kumar, M.R. Wilkins, C.L. Jones, R. L. Huhnke, Effects of cellulose, hemicellulose and lignin on thermochemical conversion characteristics of the selected biomass, Bioresour. Technol. 114 (2012) 663–669, https://doi.org/10.1016/j.biortech.2012.03.036.

[4] S.D. Stefanidis, K.G. Kalogiannis, E.F. Iliopoulou, C.M. Michailof, P.A. Pilavachi, A. A. Lappas, A study of lignocellulosic biomass pyrolysis via the pyrolysis of cellulose, hemicellulose and lignin, J. Anal. Appl. Pyrolysis 105 (2014) 143–150, https://doi.org/10.1016/j.jaap.2013.10.013.

[5] X. Zhao, L. Zhang, D. Liu, Biomass recalcitrance. Part I: the chemical compositions and physical structures affecting the enzymatic hydrolysis of lignocellulose, Biofuels, Bioprod. Bioref. 6 (2012) 465–482, https://doi.org/10.1002/bbb.1331.

[6] O. Senneca, F. Cerciello, C. Russo, A. Wütscher, M. Muhler, B. Apicella, Thermal treatment of lignin, cellulose and hemicellulose in nitrogen and carbon dioxide, Fuel 271 (2020) 117656, https://doi.org/10.1016/j.fuel.2020.117656.

[7] C. Quan, N. Gao, Q. Song, Pyrolysis of biomass components in a TGA and a fixed-bed reactor: thermochemical behaviors, kinetics, and product characterization, J. Anal. Appl. Pyrolysis 121 (2016) 84–92, https://doi.org/10.1016/j. jaap.2016.07.005.

[8] A.H. Hubble, J.L. Goldfarb, Synergistic effects of biomass building blocks on pyrolysis gas and bio-oil formation, J. Anal. Appl. Pyrolysis 156 (2021), https:// doi.org/10.1016/j.jaap.2021.105100.

[9] J. Escalante, W.H. Chen, M. Tabatabaei, A.T. Hoang, E.E. Kwon, K.Y. Andrew Lin, A. Saravanakumar, Pyrolysis of lignocellulosic, algal, plastic, and other biomass wastes for biofuel production and circular bioeconomy: a review of thermogravimetric analysis (TGA) approach, Renew. Sustain. Energy Rev. 169 (2022), https://doi.org/10.1016/j.rser.2022.112914.

[10] M. Radojević, B. Janković, D. Stojiljković, V. Jovanović, I. Čeković, N. Manić, Improved TGA-MS measurements for evolved gas analysis (EGA) during pyrolysis process of various biomass feedstocks. Syngas energy balance determination, Thermochim. Acta 699 (2021), https://doi.org/10.1016/j.tca.2021.178912.

[11] S. Singh, C. Wu, P.T. Williams, Pyrolysis of waste materials using TGA-MS and TGA-FTIR as complementary characterisation techniques, J. Anal. Appl. Pyrolysis 94 (2012) 99–107, https://doi.org/10.1016/j.jaap.2011.11.011.

[12] D. Wang, R. Xiao, H. Zhang, G. He, Comparison of catalytic pyrolysis of biomass with MCM-41 and CaO catalysts by using TGA-FTIR analysis, J. Anal. Appl. Pyrolysis 89 (2010) 171–177, https://doi.org/10.1016/j.jaap.2010.07.008.

[13] J. Fermoso, O. Mašek, Thermochemical decomposition of coffee ground residues by TG-MS: a kinetic study, J. Anal. Appl. Pyrolysis 130 (2018) 249–255, https:// doi.org/10.1016/j.jaap.2017.12.007.

[14] S. Maduskar, V. Maliekkal, M. Neurock, P.J. Dauenhauer, On the yield of levoglucosan from cellulose pyrolysis, ACS Sustain Chem. Eng. 6 (2018) 7017–7025, https://doi.org/10.1021/acssuschemeng.8b00853.

[15] S. Wang, H. Lin, L. Zhang, G. Dai, Y. Zhao, X. Wang, B. Ru, Structural characterization and pyrolysis behavior of cellulose and hemicellulose isolated

from softwood *Pinus armandii* Franch, Energy Fuels 30 (2016) 5721–5728, https:// doi.org/10.1021/acs.energyfuels.6b00650.

[16] S. Zhao, M. Liu, L. Zhao, L. Zhu, Influence of Interactions among three biomass components on the pyrolysis behavior, Ind. Eng. Chem. Res 57 (2018) 5241–5249, https://doi.org/10.1021/acs.iecr.8b00593.

[17] X. Zhou, M.W. Nolte, H.B. Mayes, B.H. Shanks, L.J. Broadbelt, Experimental and mechanistic modeling of fast pyrolysis of neat glucose-based carbohydrates. 1. Experiments and development of a detailed mechanistic model, Ind. Eng. Chem. Res 53 (2014) 13274–13289, https://doi.org/10.1021/ie502259w.

[18] L. Burhenne, J. Messmer, T. Aicher, M.P. Laborie, The effect of the biomass components lignin, cellulose and hemicellulose on TGA and fixed bed pyrolysis, J. Anal. Appl. Pyrolysis 101 (2013) 177–184, https://doi.org/10.1016/j. jaap.2013.01.012.

[19] T.J.P. Oliveira, C.R. Cardoso, C.H. Ataíde, Fast pyrolysis of soy hulls in a fluidized bed reactor: Main components of the bio-oil. Materials Science Forum, Trans Tech Publications Ltd, 2014, pp. 239–244, https://doi.org/10.4028/www.scientific.net/ MSF.802.239.

[20] A. Trubetskaya, L. von Berg, R. Johnson, S. Moore, J.J. Leahy, Y. Han, H. Lange, A. Anca-Couce, Production and characterization of bio-oil from fluidized bed pyrolysis of olive stones, pinewood, and torrefied feedstock, J. Anal. Appl. Pyrolysis 169 (2023), https://doi.org/10.1016/j.jaap.2022.105841.

[21] R. Liu, C. Deng, J. Wang, Fast pyrolysis of corn straw for bio-oil production in a bench-scale fluidized bed reactor, Energy Sources, Part A: Recovery, Util. Environ. Eff. 32 (2010) 10–19, https://doi.org/10.1080/15567030802094037.

[22] J. Alvarez, G. Lopez, M. Amutio, J. Bilbao, M. Olazar, Bio-oil production from rice husk fast pyrolysis in a conical spouted bed reactor, Fuel 128 (2014) 162–169, https://doi.org/10.1016/j.fuel.2014.02.074.

[23] R. Aguado, M. Olazar, M.J. San José, G. Aguirre, J. Bilbao, Pyrolysis of sawdust in a conical spouted bed reactor. Yields and product composition, Ind. Eng. Chem. Res 39 (2000) 1925–1933, https://doi.org/10.1021/ie990309v.

[24] S. Hameed, A. Sharma, V. Pareek, H. Wu, Y. Yu, A review on biomass pyrolysis models: kinetic, network and mechanistic models, Biomass-.-. Bioenergy 123 (2019) 104–122, https://doi.org/10.1016/j.biombioe.2019.02.008.

[25] E. Ranzi, A. Cuoci, T. Faravelli, A. Frassoldati, G. Migliavacca, S. Pierucci, S. Sommariva, Chemical kinetics of biomass pyrolysis, Energy Fuels 22 (2008) 4292–4300, https://doi.org/10.1021/ef800551t.

[26] E. Ranzi, P.E.A. Debiagi, A. Frassoldati, Mathematical modeling of fast biomass pyrolysis and bio-oil formation. note ii: secondary gas-phase reactions and bio-oil formation, ACS Sustain Chem. Eng. 5 (2017) 2882–2896, https://doi.org/10.1021/ acssuschemeng.6b03098.

[27] E. Ranzi, P.E.A. Debiagi, A. Frassoldati, Mathematical modeling of fast biomass pyrolysis and bio-oil formation. note i: kinetic mechanism of biomass pyrolysis, ACS Sustain Chem. Eng. 5 (2017) 2867–2881, https://doi.org/10.1021/ acssuschemeng.6b03096.

[28] P. Debiagi, G. Gentile, A. Cuoci, A. Frassoldati, E. Ranzi, T. Faravelli, A predictive model of biochar formation and characterization, J. Anal. Appl. Pyrolysis 134 (2018) 326–335, https://doi.org/10.1016/j.jaap.2018.06.022.

[29] T. Faravelli, A. Frassoldati, G. Migliavacca, E. Ranzi, Detailed kinetic modeling of the thermal degradation of lignins, Biomass-.-. Bioenergy 34 (2010) 290–301, https://doi.org/10.1016/j.biombioe.2009.10.018.

[30] T. Faravelli, A. Frassoldati, E. Barker Hemings, E. Ranzi, Multistep kinetic model of biomass pyrolysis, in: F. Battin-Leclerc, M.; Simmie; John, Blurock; Edward (Eds.), Cleaner Combustion. Green Energy and Technology, Springer, London, 2013, pp. 111–139, https://doi.org/10.1007/978-1-4471-5307-8_5.

[31] E. Ranzi, M. Corbetta, F. Manenti, S. Pierucci, Kinetic modeling of the thermal degradation and combustion of biomass, Chem. Eng. Sci. 110 (2014) 2–12, https:// doi.org/10.1016/j.ces.2013.08.014.

[32] S. Zellagui, C. Schönnenbeck, N. Zouaoui-Mahzoul, G. Leyssens, O. Authier, E. Thunin, L. Porcheron, J.F. Brilhac, Pyrolysis of coal and woody biomass under N2 and CO2 atmospheres using a drop tube furnace - experimental study and kinetic modeling, Fuel Process. Technol. 148 (2016) 99–109, https://doi.org/ 10.1016/j.fuproc.2016.02.007.

[33] R. Lemaire, W. Wang, S. Menanteau, Kinetic modeling of the devolatilization of pulverized coal, poplar wood, and their blends in a thermogravimetric analyzer and a flat flame reactor, ACS Omega 8 (2023) 29455–29467, https://doi.org/ 10.1021/acsomega.3c03110.

[34] J.L. Banyasz, S. Li, J. Lyons-Hart, K.H. Shafer, Gas evolution and the mechanism of cellulose pyrolysis, Fuel 80 (2001) 1757–1763.

[35] A.G.W. Bradbury, Y. Sakai, F. Shafizadeh, A Kinetic Model for Pyrolysis of Cellulose, J. Appl. Polym. Sci. 23 (1979) 3271–3280.

[36] J.L. Banyasz, S. Li, J.L. Lyons-Hart, K.H. Shafer, Cellulose pyrolysis: the kinetics of hydroxyacetaldehyde evolution, J. Anal. Appl. Pyrolysis 57 (2001) 223–248 (www.elsevier.com/locate/jaap).

[37] Z. Luo, S. Wang, Y. Liao, K. Cen, Mechanism study of cellulose rapid pyrolysis, Ind. Eng. Chem. Res 43 (2004) 5605–5610, https://doi.org/10.1021/ie030774z.

[38] F. Shafizadeh, Introduction to pyrolysis of biomass, J. Anal. Appl. Pyrolysis 3 (1982) 283–305.

[39] A. Cuoci, A. Frassoldati, T. Faravelli, E. Ranzi, OpenSMOKE++: An object-oriented framework for the numerical modeling of reactive systems with detailed kinetic mechanisms, Comput. Phys. Commun. 192 (2015) 237–264, https://doi.org/ 10.1016/j.cpc.2015.02.014.

[40] D. Fabbri, C. Torri, V. Baravelli, Effect of zeolites and nanopowder metal oxides on the distribution of chiral anhydrosugars evolved from pyrolysis of cellulose: An analytical study, J. Anal. Appl. Pyrolysis 80 (2007) 24–29, https://doi.org/ 10.1016/j.jaap.2006.12.025.

[41] Z. Zhang, M. Zhu, D. Zhang, A Thermogravimetric study of the characteristics of pyrolysis of cellulose isolated from selected biomass, Appl. Energy 220 (2018) 87–93, https://doi.org/10.1016/j.apenergy.2018.03.057.

[42] M.O. Adenson, M.D. Kelley, O.O. Elkelany, J.J. Biernacki, Y.W. Liu, Kinetics of cellulose pyrolysis: ensuring optimal outcomes, Can. J. Chem. Eng. 96 (2018) 926–935, https://doi.org/10.1002/cjce.23060.

[43] Y. Zheng, L. Tao, X. Yang, Y. Huang, C. Liu, Z. Zheng, Study of the thermal behavior, kinetics, and product characterization of biomass and low-density polyethylene co-pyrolysis by thermogravimetric analysis and pyrolysis-GC/MS, J. Anal. Appl. Pyrolysis 133 (2018) 185–197, https://doi.org/10.1016/j.jaap.2018.04.001.

[44] H. Zhou, Y. Long, A. Meng, S. Chen, Q. Li, Y. Zhang, A novel method for kinetics analysis of pyrolysis of hemicellulose, cellulose, and lignin in TGA and macro-TGA, RSC Adv. 5 (2015) 26509–26516, https://doi.org/10.1039/c5ra02715b.

[45] A. Anca-Couce, C. Tsekos, S. Retschitzegger, F. Zimbardi, A. Funke, S. Banks, T. Kraia, P. Marques, R. Scharler, W. de Jong, N. Kienzl, Biomass pyrolysis TGA assessment with an international round robin, Fuel 276 (2020) 118002, https://doi.org/10.1016/j.fuel.2020.118002.

[46] I. Milosavljevic, E.M. Suuberg, Cellulose thermal decomposition kinetics: global mass loss kinetics, Ind. Eng. Chem. Res 34 (1995) 1081–1091, https://doi.org/10.1021/ie00043a009.

[47] D.K. Shen, S. Gu, The mechanism for thermal decomposition of cellulose and its main products, Bioresour. Technol. 100 (2009) 6496–6504, https://doi.org/10.1016/j.biortech.2009.06.095.

[48] A. Broido, M.A. Nelson, Char yield on pyrolysis of cellulose, Combust. Flame 24 (1975) 263–268.

[49] D.P. Koullas, E. Lois, E.G. Koukios, Effect of physical pretreatments on the prepyrolytic behaviour of lignocellulosics, Biomass-.-. Bioenergy I (1991) 199–206.

[50] D.F. Arseneau, Competitive reactions in the thermal decomposition of cellulose, Can. J. Chem. 49 (1971) 632.

[51] F.X. Collard, J. Blin, A review on pyrolysis of biomass constituents: mechanisms and composition of the products obtained from the conversion of cellulose, hemicelluloses and lignin, Renew. Sustain. Energy Rev. 38 (2014) 594–608, https://doi.org/10.1016/j.rser.2014.06.013.

[52] T.E. McGrath, W.G. Chan, R. Hajaligol, Low temperature mechanism for the formation of polycyclic aromatic hydrocarbons from the pyrolysis of cellulose, v. 66, p. 51-70, 2003., J Anal Appl Pyrolysis, J. Anal. Appl. Pyrolysis 66 (2003) 51–70.

[53] S. Vyazovkin, K. Chrissafis, M.L. Di Lorenzo, N. Koga, M. Pijolat, B. Roduit, N. Sbirrazzuoli, J.J. Suñol, ICTAC Kinetics committee recommendations for collecting experimental thermal analysis data for kinetic computations, Thermochim. Acta 590 (2014) 1–23, https://doi.org/10.1016/j.tca.2014.05.036.

[54] H. Wang, Q. Yao, C. Wang, B. Fan, Y. Xiong, Y. Chen, Q. Sun, C. Jin, Z. Ma, New Insight on Promoted thermostability of poplar wood modified by MnFe2O4 nanoparticles through the pyrolysis behaviors and kinetic study, Sci. Rep. 7 (2017), https://doi.org/10.1038/s41598-017-01597-4.

[55] J. Kristanto, A.F. Daniyal, D.Y. Pratama, I.N.M. Bening, L. Setiawan, M.M. Azis, S. Purwono, Kinetic study on the slow pyrolysis of isolated cellulose and lignin

[56] from teak sawdust, Thermochim. Acta 711 (2022), https://doi.org/10.1016/j.tca.2022.179202.

[56] M.E. Eugenio, M. Ruiz-Montoya, R. Martín-Sampedro, D. Ibarra, M.J. Díaz, Influence of cellulose characteristics on pyrolysis suitability, Processes 9 (2021), https://doi.org/10.3390/pr9091584.

[57] Z. Lei, S. Wang, H. Fu, W. Gao, B. Wang, J. Zeng, J. Xu, Thermal pyrolysis characteristics and kinetics of hemicellulose isolated from Camellia Oleifera Shell, Bioresour. Technol. 282 (2019) 228–235, https://doi.org/10.1016/j.biortech.2019.02.131.

[58] T. Ozawa, A new method of analyzing thermogravimetric data, Bull. Chem. Soc. Jpn 38 (1965) 1881–1886.

[59] A.K. Burnham, X. Zhou, L.J. Broadbelt, Critical review of the global chemical kinetics of cellulose thermal decomposition, Energy Fuels 29 (2015) 2906–2918, https://doi.org/10.1021/acs.energyfuels.5b00350.

[60] A. Cuoci, T. Faravelli, A. Frassoldati, S. Granata, G. Migliavacca, E. Ranzi, S. Sommariva, A General Mathematical Model of Biomass Devolatilization Note 1. Lumped kinetic models of cellulose, hemicellulose and lignin, in: 30th Meeting of the Italian Section of The Combustion Institute, 2007.

[61] K.B. Ansari, J.S. Arora, J.W. Chew, P.J. Dauenhauer, S.H. Mushrif, Fast pyrolysis of cellulose, hemicellulose, and lignin: effect of operating temperature on bio-oil yield and composition and insights into the intrinsic pyrolysis chemistry, Ind. Eng. Chem. Res 58 (2019) 15838–15852, https://doi.org/10.1021/acs.iecr.9b00920.

[62] C. Zhao, E. Jiang, A. Chen, Volatile production from pyrolysis of cellulose, hemicellulose and lignin, J. Energy Inst. 90 (2017) 902–913, https://doi.org/10.1016/j.joei.2016.08.004.

[63] N. Worasuwannarak, T. Sonobe, W. Tanthapanichakoon, Pyrolysis behaviors of rice straw, rice husk, and corncob by TG-MS technique, J. Anal. Appl. Pyrolysis 78 (2007) 265–271, https://doi.org/10.1016/j.jaap.2006.08.002.

[64] G. SriBala, D.C. Vargas, P. Kostetskyy, R. Van de Vijver, L.J. Broadbelt, G.B. Marin, K.M. Van Geem, New perspectives into cellulose fast pyrolysis kinetics using a Py-GC × GC-FID/MS system, ACS Eng. Au 2 (2022) 320–332, https://doi.org/10.1021/acsengineeringau.2c00006.

[65] X. Zhou, M.W. Nolte, B.H. Shanks, L.J. Broadbelt, Experimental and mechanistic modeling of fast pyrolysis of neat glucose-based carbohydrates. 2. Validation and Evaluation of theMechanistic Model, Ind. Eng. Chem. Res 53 (2014) 13290–13301, https://doi.org/10.1021/ie502259w.

[66] F. Shafizadeh, R.H. Furneaux, T.G. Cochran, J.P. Scholl, Y. Sakai, Production of levoglucosan and glucose from pyrolysis of cellulosic materials, J. Appl. Polym. Sci. 23 (1979) 3525–3539, https://doi.org/10.1002/app.1979.070231209.

[67] H. Kawamoto, Review of Reactions and Molecular Mechanisms in Cellulose Pyrolysis, Curr Org Chem 20 (2016) 2444–2457. http://hdl.handle.net/2433/240620http://www.eurekaselect.com/.

[68] J. Lédé, Cellulose pyrolysis kinetics: an historical review on the existence and role of intermediate active cellulose, J. Anal. Appl. Pyrolysis 94 (2012) 17–32, https://doi.org/10.1016/j.jaap.2011.12.019.

[69] J. Schroeter, F. Felix, Melting cellulose, Cellulose 12 (2005) 159–165, https://doi.org/10.1007/s10570-004-0344-3.